The mechanism of intermediate temperature embrittlement of cast irons by magnesium

R. González-Martínez[1], J. Sertucha[1], Jacques Lacaze[2]

1 AZTERLAN, Basque Research and Technology Alliance (BRTA), Durango, Spain
2 CIRIMAT, Université de Toulouse, BP 44362. F-31030 Toulouse, France

Abstract

Metallic alloys such as steels and nickel-based alloys are potentially vulnerable to high-temperature brittleness in the range of 500°C to 900°C that results in a loss of ductility. Ferritic spheroidal graphite cast irons show similar loss of ductility at temperatures between 350°C and 500°C, suggesting the term intermediate temperature brittleness. Previous works have shown that sulfur and magnesium are detrimental while phosphorus added at a reasonable level is beneficial in preventing loss of ductility in ferritic spheroidal graphite castings.

In order to clarify the role of magnesium, a ferritic spheroidal graphite cast iron with high silicon content and low sulfur and phosphorus contents was subjected to tensile tests between room temperature and 650°C. It was found to be susceptible to embrittlement at intermediate temperatures around 400°C. MgO precipitates were observed on the fracture surface, which increased in size with test temperature, confirming the role of the environment that was reported by previous researchers. This finding is cross-checked with the results of the literature and allows us to propose a scheme for intermediate temperature embrittlement of ferritic spheroidal graphite iron.

Keywords

Spheroidal graphite cast iron; intermediate temperature brittleness; magnesium; oxygen

Corresponding author: Jacques Lacaze, CIRIMAT, 4 allée Monso, CS 44362, 31030 Toulouse cedex, France. Tel. 33+534323403, Fax: 33+534323399, e-mail:Jacques.lacaze@ensiacet.fr

1. Introduction

Nickel-based alloys and steels exhibit a ductility trough between 500°C and 1000°C, as studied by Lei Zheng et al [1] for nickel-based alloys and Lankford [2] and Mintz and Crowther [3, 4] for steels in connection with continuous casting. Steels also exhibit low temperature brittleness with a transition temperature from ductile to brittle fracture (TTDB) that varies from about -100°C to about +100°C depending on the alloy composition and process parameters. In particular, it is known that the segregation of sulfur and phosphorus at the grain boundaries results in a shift of the TTDB to higher temperatures, making many steels susceptible to temper embrittlement. This segregation decreases grain boundary strength that favors intergranular fracture. In the high-temperature regime, the ductility trough is related to intergranular fracture, but is generally not due to grain boundary segregation, but depends on precipitation.

Ferritic spheroidal graphite cast irons (SGI) are similar to steels in that they exhibit low temperature brittleness with the TTDB located between -50°C and room temperature (RT) or slightly above, and a ductility trough in the temperature range of 300°C to 500°C. The latter is associated with the occurrence of intergranular fracture (IG) and has been referred to as 673 K embrittlement by Yanasigawa and Lui [5] and high temperature embrittlement by Wright and Farrell [6]. In the present work, we will adopt the name intermediate temperature embrittlement (ITB) which has also been proposed and is more appropriate for the temperature range involved. Wright and Farrell [6] demonstrated that ITB in SGI increases with increasing sulfur and magnesium content and suggested a mechanism based on sulfur diffusion at grain boundaries. In this temperature range, phosphorus also tends to segregate at grain boundaries in SGI, as confirmed by Chen et al [7, 8] using Auger electron spectroscopy. However, these authors came to the conclusion of the role of MgO particles on the fracture, in agreement with other works [5, 9, 10, 11]. In addition, phosphorus has been shown to be beneficial in decreasing the incidence of ITB in alloys with magnesium/phosphorus ratios less than 1.5 [10, 12]. Similarly, ferrite grain size refinement is effective in reducing the risk of brittle fracture and loss of ductility [5, 13].

Experimentally, ITB is best evidenced by the abrupt decrease in the temperature range 300-500°C in the elongation at rupture, A, or the decrease in the reduction area at rupture, RA. It has been shown quantitatively by Iwabuchi and Kobayashi [14, 15] that these two quantities are nearly equal and thus can be considered equivalent in practice, which will be used here to report data from various sources. Interestingly, although most often studied by tensile testing, this embrittlement also plays an important role in cyclic loading, as revealed by low-cycle fatigue and rotating bending fatigue data [6, 10, 16].

Not all ferritic SGIs are sensitive to ITB as shown in Figure 1 using data from Wright and Farrell [6] for SGIs with 2.2-2.6 wt% Si (more details are given in the Appendix A). At 400-425°C, Figure 1 shows that RA falls below 10% for alloys B, E, and G but not for alloy H (solid triangles). This alloy H had been spheroidized with low magnesium addition, leading to a residual magnesium content of 0.023 wt%, less than half the amount of the other three alloys.

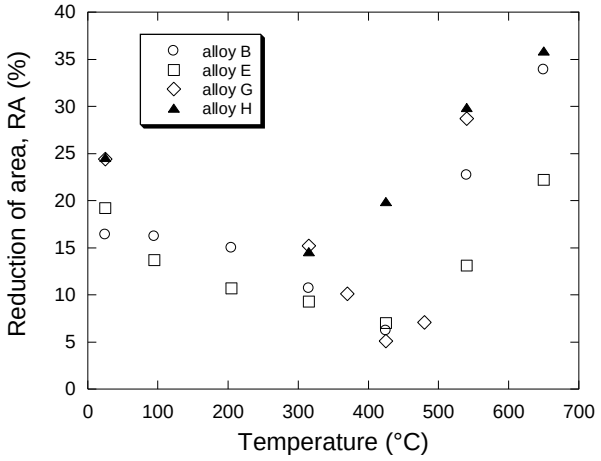

Figure 1. Evolution with temperature of the reduction of area at rupture for the alloys B, E, G and H studied by Wright and Farrell [6]. Whenever there were duplicate values, this is the mean value that is plotted.

Wright and Farrell confirmed that embrittlement is associated with IG fracture and showed that it initiates on micro-porosities. The authors also noted that low ductility at 425°C, i.e., a low RA value, is associable with high magnesium and sulfur contents, and drew a parallel with ferritic steels by considering sulfur to be the embrittler. On the other hand, Iwabuchi and Kobayashi [15] concluded that IG

fracture occurs due to segregation at the grain boundaries and associated it with a %Mg/%P ratio greater than 1.5 as proposed by Takanezawa et al. [12], where %Mg and %P are the magnesium and phosphorus contents of the alloy expressed in wt%.

Most of the studies on ITB in spheroidal graphite cast irons were concerned with alloys that had been heat-treated to ensure a fully ferritic matrix. However, high-silicon SGI do not need such a heat-treatment that is known to favor grain boundary segregation of impurities such as sulfur and phosphorus. In spite of this, our research work that was dedicated to the characterization of the effect of temperature on the mechanical properties of a high-silicon SGI showed it to be sensitive to ITB in the as-cast state. This report presents the results of the mechanical tests that were performed from room temperature to 650°C and the metallographic characterization of the fracture surfaces. This information and literature data are compared, and the discussion leads to propose a scheme for intermediate temperature embrittlement of as-cast ferritic spheroidal graphite cast irons

2. Experimental details.

The melt was prepared in a medium frequency furnace (250Hz, 100kW) 100 kg in capacity with a metallic charge consisting of 50% low alloyed steel scrap and 50 % low alloyed pig iron. Once melting was completed, the carbon and silicon contents were adjusted by adding high purity graphite ($>$ 99.0 wt% carbon) and a FeSi75 alloy (Si=74.8, Ca=0.30, Al=0.76, C=0.10 and Fe balance, wt%), respectively. A verification of the chemical composition was subsequently made and then the melt temperature was increased to 1510°C–1520°C and hold at that temperature for successive castings. The spheroidizing treatment was performed with magnesium, following the so-called sandwich method by transferring 50 kg of the prepared alloy to a ladle where FeSiMg alloy (grain size 5–25 mm, Si=46.60, Mg=6.00, Ca=0.96, Al=0.71 and rare earth RE=0.92, Fe balance, wt%) had been positioned in an amount of 0.6 kg (1.2 wt% of the batch weight) and then covered with steel scrap (grain size 5-15 mm). After completion of the spheroidizing reaction, the alloy was skimmed and finally cast. The operation was repeated with the remaining melt to fill the rest of the molds.

The molds were standard Y2 keel-blocks (EN-1563) manufactured with chemical bonded sand whose bottom leg (40x150x25 cm) is the useable part because generally devoid of porosity and inclusions. Each mold contained one cavity in which 14 g (0.20 wt% of the total weight of the cast iron poured in the mold) of a commercial inoculant (grain size 0.2–0.5 mm, Si=69.9, Al=0.93, Ca=1.38, Bi=0.49, RE=0.37and Fe balance, wt%) was added before pouring the melt. After cooling of the castings, the keel-blocks were removed from the molds and cleaned, and two tensile specimens were machined out from the bottom leg (total length of 115 mm, gage of 50 mm in length and 10 mm in diameter).

The tensile parameters, namely the ultimate tensile strength (UTS) and the elongation at rupture (A) were measured using an MTS 810 tensile testing equipment at a constant displacement rate of 0.90 mm/min, thus corresponding to an initial strain rate of $3 \cdot 10^{-4}$ s^{-1}. Duplicate tensile tests were performed at RT, 100°C, 350°C, 450°C, 475°C, 500°C and 650°C. For temperature testing, use has been made of a MTS 653 furnace attached to the tensile equipment, and the samples were hold for 10 min at the selected temperature before testing. Three thermocouples located along the gage section were used to monitor the sample temperature and limit the temperature fluctuations within $\pm$3°C. Once the tensile test had been completed, one of the fracture surfaces was analyzed by scanning electron microscopy (SEM) using a Quanta 200 Carl Zeiss Ultraplus operated at 20 kV. Local chemical microanalyses were carried out with an energy dispersive spectrometer (EDS) X-max 20 Oxford that the SEM is equipped with.

The quality of the spheroidizing treatment has been checked by light optical metallography on one tensile specimen tested at RT. Figure 2 shows a fairly even distribution of well-rounded graphite spheroids. Finally, one piece of this tensile specimen was used for chemical analysis whose results are listed in Table 1.

Table 1. Chemical composition (wt.%) of the cast alloy.

C	Si	Mn	P	S	Cu	Cr	Ni	Ti	Mg	Ce	La	Sb
3.00	4.99	0.20	0.012	0.007	0.036	0.040	0.061	0.016	0.038	0.0066	0.0033	0.0059

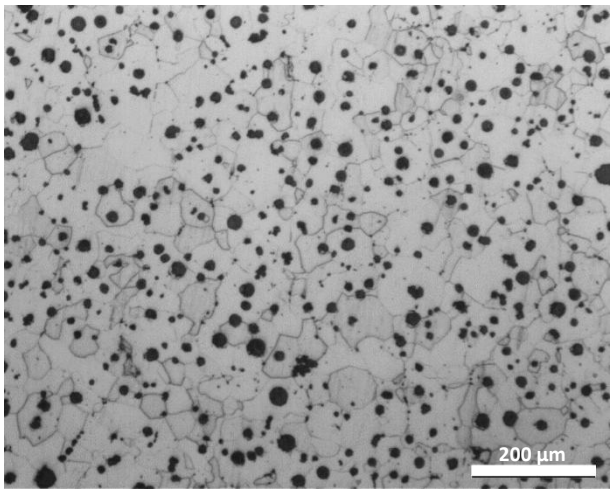

Figure 2. Light optical micrograph of the microstructure of the cast alloys.

3. Results.

The tensile tests curves of duplicates were quite reproducible and one for each of the test temperatures has been plotted in Figure 3. The values of UTS and A for all tests, including the duplicates, are listed in Table 2. In some cases, the rupture occurred outside the grips of the extensometer in which case A was not reported. The alloy showed the maximum UTS values at room temperature (RT) while the A values at 8.8% and 13.1% are in the high range of previously reported data on SGI with about 5 wt.% Si [17]. When the testing temperature increased to 100°C, the UTS values decreased a little and the A values increased slightly over the RT results at 14.3% and 15.9% that possibly indicates that the chemical ordering of ferrite already started to decrease. At 350 °C and above, the UTS values continuously decreased while A was observed to fall below 5% from 350°C to 500°C and then to increase to quite high values at 650°C. The alloy thus appeared sensitive to ITB with a ductility trough between 350°C and 500°C with a possible minimum at 475°C.

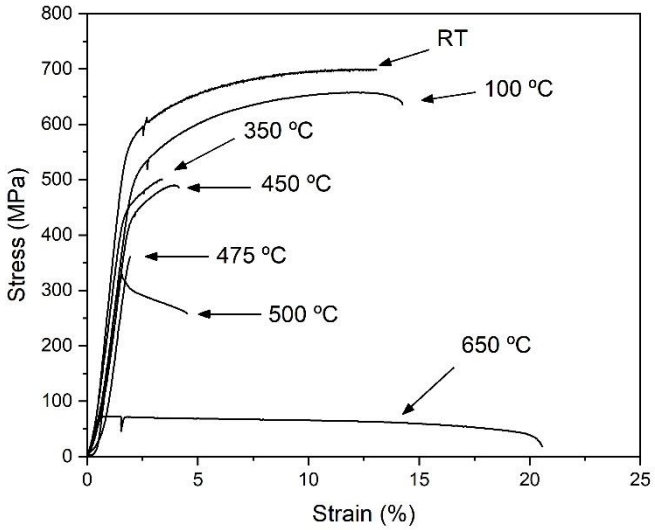

Figure 3. Tensile strain-stress curves at the various testing temperatures.

Table 2. Results from duplicate tensile tests (UTS and A) conducted at room temperature (RT), 100°C, 350°C, 450°C, 475°C, 500°C and 650°C.

Test Temperature (°C)	UTS (MPa)	A (%)
RT	700	13.1
RT	691	8.8
100	652	15.9
100	658	14.3
350	425	---
350	501	3.4
450	490	---
450	490	4.2
475	230	---
475	361	---
500	328	4.5
500	328	---
650	77	23.1
650	73	20.5

In Figure 4, A values from the present work are plotted as a function of the testing temperature with solid symbols that illustrate the ductility trough between 350°C and 500°C. For comparison with literature, data for SGI with silicon content higher than 3.5 wt.% were selected [10, 11, 18], including a molybdenum alloyed SiMo SGI [19]. As seen with Figure 1 for low silicon SGI, it is noted that some high silicon alloys are

immune to ITB. These alloys are those with low magnesium content and, generally, a low %Mg/%P ratio in agreement with results by Takanezawa et al. [12] and Cheng et al. [20]. In the same line, it is noticeable that Chen et al. [8] suppressed ITB in SGI containing 3.9 wt.% Si by spheroidizing with Ce and no Mg, and that even a 0.011 wt.% residual Mg was sufficient to generate ITB.

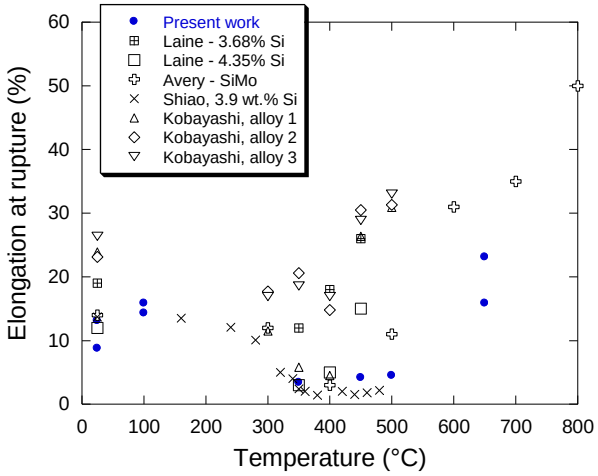

Figure 4. Variation of A with temperature for the present study and works on high silicon SGI (with silicon content higher than 3.5 wt.%) by Kobayashi et al. [10], Shiao et al. [11] and Laine et al. [18], as well as on a SiMo SGI [19].

An interesting feature that Wright and Farrell [6] reported is that the ductility loss is much less apparent when considering the evolution of UTS as function of temperature because it continuously decreases. This means that UTS values of samples showing or not IG fracture should be comparable. In order to compare literature results for cast irons with differing silicon contents, Figure 5 shows the evolution of UTS after normalizing each series of data with their maximum value at room temperature. Results for low and high silicon contents are reported with open and solid symbols, respectively, with literature data from Wright and Farrell [6], Iwabuchi et al. [15] and Laine et al. [18]. Data for the SiMo SGI studied by Avery et al. [19] are plotted with a large plus sign as in Figure 4.

It is seen in Figure 5 that all UTS values show the same temperature evolution within a reasonable scatter band, with some of the values of the present study appearing however quite low. Though not further investigated, this could be related to the fact that there was no heat-treatment applied to the present material. It is noticeable that

UTS processes in two steps at increasing temperature, with a slow and then steeper decrease below and beyond a critical temperature of about 300°C. Such a behavior had already been noticed for a SiMo SGI [21] and is here extended to the whole silicon range used in SGI.

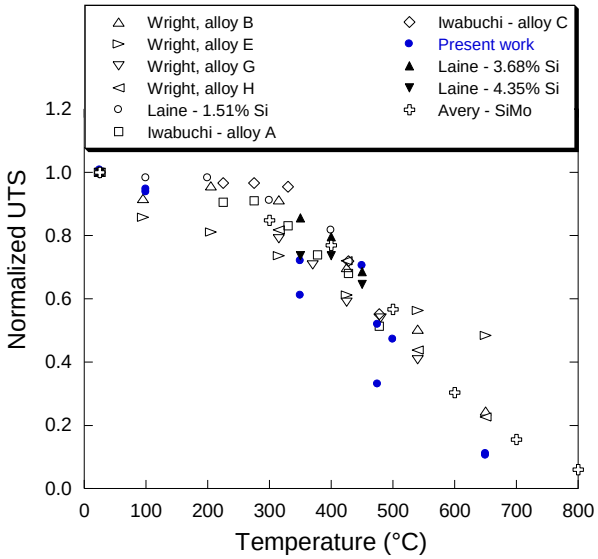

Figure 5. Variation with temperature of the normalized value of UTS for low (open symbols) and high (solid symbols) silicon SGI. Literature data are from Wright and Farrell [6], Iwabuchi et al. [15], Laine et al. [18] and Avery et al. [19]. Normalization was carried out using the RT value for each of the series of results.

SEM characterization of the rupture surfaces was systematically carried out and Figure 6 presents a representative micrograph for six test temperatures. At room temperature, Figure 6a shows that the alloy exhibited mainly cleavage fracture with some areas of intergranular fracture such as the one indicated with the arrow. At 100 ºC, the fracture surface was very similar to that at room temperature, only a slight increase of the ductile fracture area was observed. On the fracture surface of the material tested at 350 °C (Figure 6b), both an increase of the area of intergranular fracture and a change from cleavage to ductile fracture are observed. With further increase in testing temperature up to 450°C (Figure 6c), 475°C (Figure 6d) and 500°C (Figure 6e), the intergranular fracture area increased further and occupied most of the surface at 475°C. At 500ºC, the fracture started switching from intergranular to ductile fracture with the apparition of areas covered with small cupules (see later, Figure 8). Finally, the samples tested at 650°C exhibited a fully

ductile fracture (Figure 6f) with much larger cupules containing one or more graphite spheroids.

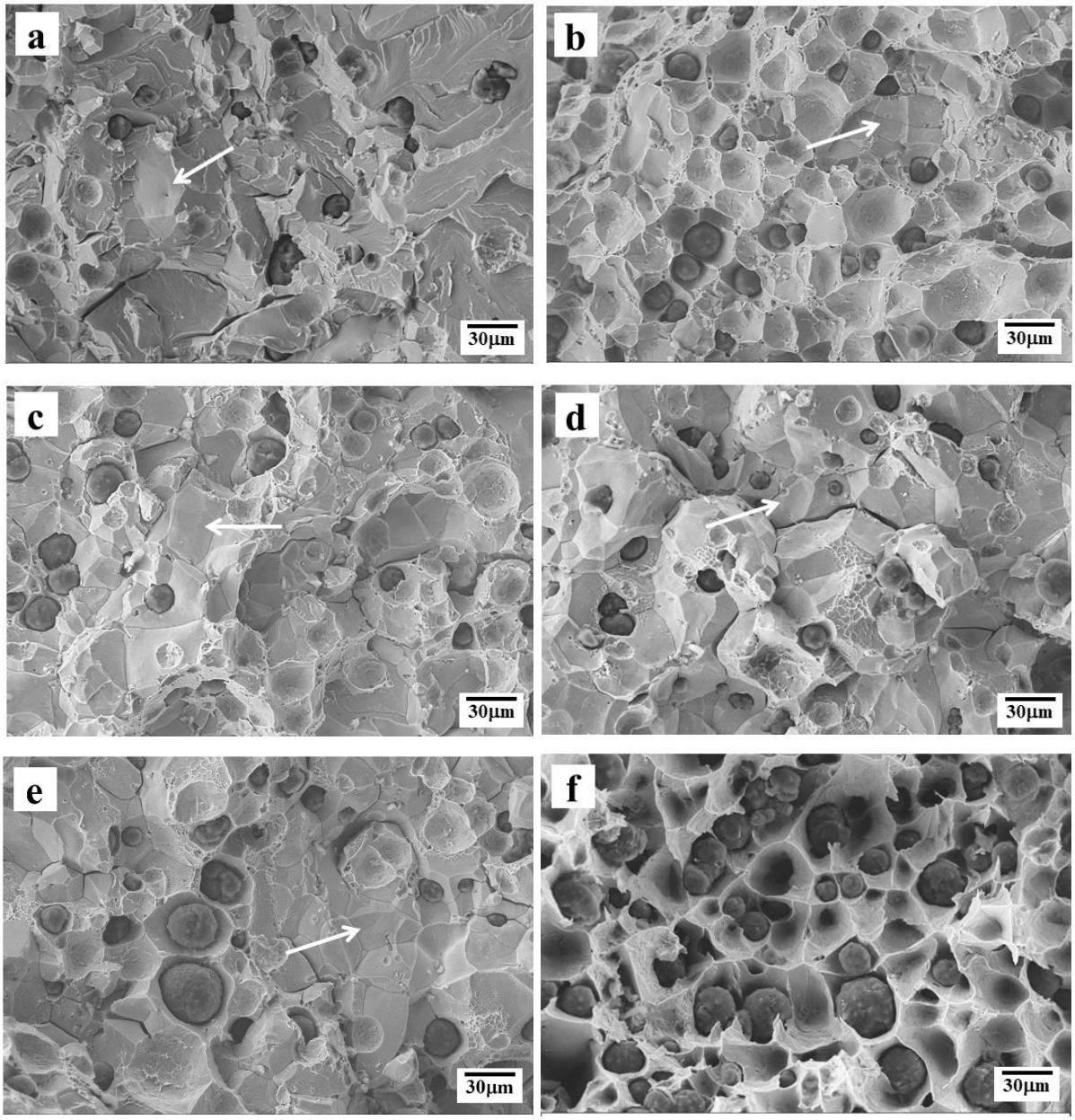

Figure 6. SEM micrograph of the fracture surface at room temperature (a), 350°C (b), 450°C (c), 475°C (d), 500°C (e) and 650°C (f). The arrows indicate intergranular facet.

Detailed observation of the ruptured surfaces evidenced the presence of particles on the IG facets as exemplified with the few micrographs in Figure 7. After testing at RT, the particles that are observed are very small; see Figure 7a and the enlarged view in Figure 7b. Already after testing at 100°C, Figure 7c and 7d, many more and larger

particles could be noticed. The surface of the sample tested at 450°C was found to be covered by numerous hemispherical aggregates, typically 0.5 µm in size, as seen in Figure 7e and 7f. Note that care was taken to have the micrographs in Figure 7a, 7c and 7e at exactly the same enlargement so as to evidence the dramatic increase in the size of the precipitates as the test temperature increased.

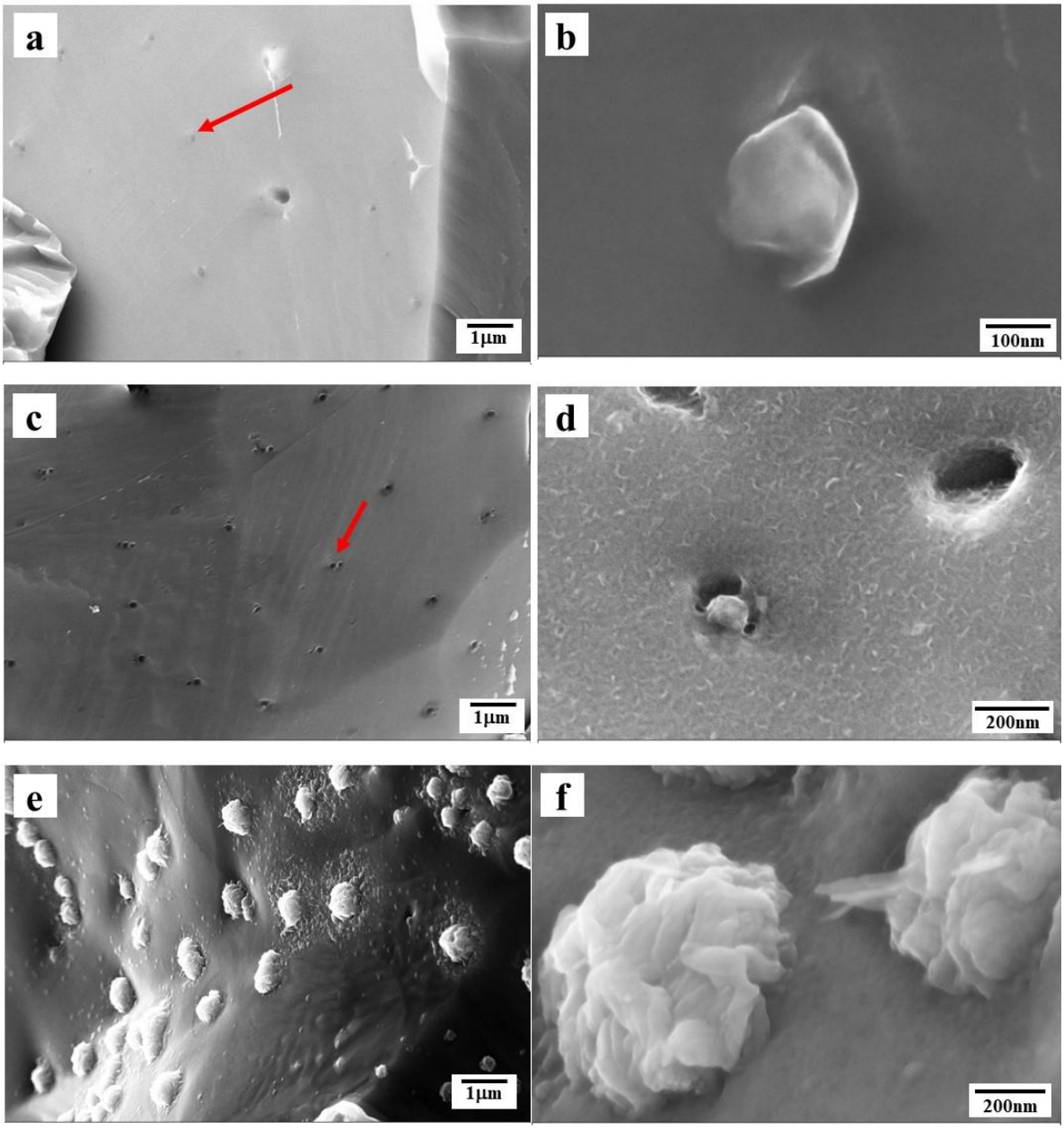

Figure 7. SEM micrographs of IG facets after fracture at room temperature (a), 100°C (c) and 450°C (e). Note that the micrographs a, c and e are at the same enlargement, and that b, d and f are details of a, c and e, respectively. The arrow in a and c points to the precipitate seen in the enlarged view, b and d respectively.

EDS spectra (see examples in Appendix B) showed these particles to contain high levels of Mg and O, and thus certainly to be MgO precipitates such as those reported by several authors, e.g. Chen et al. [7]. However, the present results show that these precipitates are very small and few in number in the as-cast state. This is only when the material is heated that numerous MgO particles precipitate and grow to a significant size in relation with the test temperature. This implies diffusion of oxygen from the ambient air into the material, certainly mostly through grain boundaries as the process is anyway quite rapid. It will be seen in the discussion that this finding is much in line with other experimental observations reported in the literature.

Figure 8a and the enlargement in Figure 8b show details of the ductile area in the sample tested at 500°C. As noted above, the cupules are very small and are seen here to be associated with particles closely resembling MgO precipitates, which is confirmed by the EDS spectrum in Figure B3 in Appendix B. This strongly suggests that the rupture there started from a grain boundary covered with MgO particles, but evolved as apparently a ductile fracture because of the increased softness of the matrix at that temperature. A trial at slightly higher temperature, which was not carried out, would certainly show that an extended part of the rupture surface would be similar with small cupules containing MgO particles.

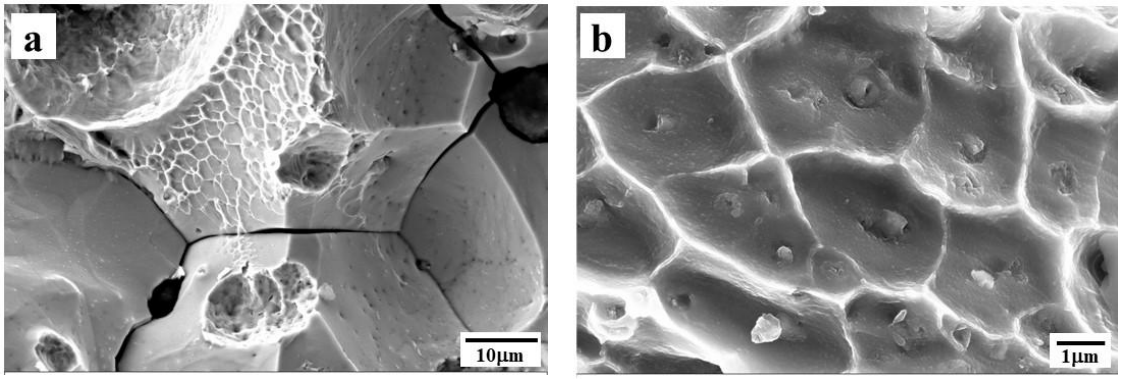

Figure 8. SEM micrographs of the fracture surface of a sample tested at 500°C. b shows detail of a.

4. Discussion

This discussion has two aspects. First, it describes an attempt to rationalize the possible effects of S, Mg, and P by confronting numerous data from the literature. Second, experimental evidences are detailed that lead to propose a mechanism for ITB in SGI.

4.1 Review of S, Mg and P effects on ITB

Instead of using the quantity (%Mg+4.5·%S) previously proposed to account for the detrimental effect of both sulfur and magnesium [22], the product %Mg·%S was considered. More precisely, it was realized that the curve separating alloys showing ITB from those that do not in the work by Wright and Farrell [6] can be represented as $\%Mg \cdot \%S = 2.3 \cdot 10^{-4}$ $(wt.\%)^2$ for sulfur content between 0.001and 0.01 wt.%. On the other hand, the ratio %Mg/%P appears well suited for rationalizing the beneficial effect of phosphorus over magnesium [10, 12]. Figure 9 is a plot of %Mg·%S values versus %Mg/%P values for a number of literature results with solid and open symbols representing respectively alloys showing or not IG fracture at 400-425°C. These results are from:

- Wright and Farrell [6], selecting only those alloys that had graphite with high nodularity (see Appendix A for details).
- Iwabuchi and Kobayashi [15].
- other works, meaning results from Chen et al. [8], Yanagisawa and Lui [5], Kobayashi et al. [10], Takanezawa et al. [23] and Li and Sloss [22].

To classify the literature data, IG has been considered when elongation at rupture or the reduction of area falls below 10%, while a mostly ductile fracture was assumed if above. It is clear that the transition may be at up to 12-13%, see for example the results by Chao et al. [13]. On the whole, Figure 9 confirms that both low %Mg/%P and %Mg·%S values are favorable for making SGI immune to ITB. This has been emphasized by drawing the rectangle at the bottom left of the graph in which mostly alloys that show no IG at 400-425°C are found. The right boundary of the rectangle was set at the critical value of 1.5 that was mentioned above, and the upper boundary at $2.3 \cdot 10^{-4}$ $(wt.\%)^2$ in agreement with Wright and Farrell data. There are however some observations to be made about this graph:

- a number of results from Wright and Farrell are outside to the right of the rectangle, which may be due to the selected value of 10% that might be underestimated.
- In the other way but not appearing in figure 9, Cheng et al. [20] and Yanagisawa et al. [24] reported results suggesting a lower critical value of %Mg/%P at 1 to 1.1.
- The horizontal arrow points to alloy i of Yanagisawa and Lui [5] that showed IG when having large ferrite grains and no IG with small ferrite grains. This alloy is located far from the origin of the graph but it was noticed it contained quite a large amount of manganese at 0.39 wt.%. Manganese may have tightened up much of the sulfur as MnS, which means that this point should probably be better located closer to the horizontal axis. This suggests that the sulfur content should be corrected to account for MnS precipitation in a more refined analysis.

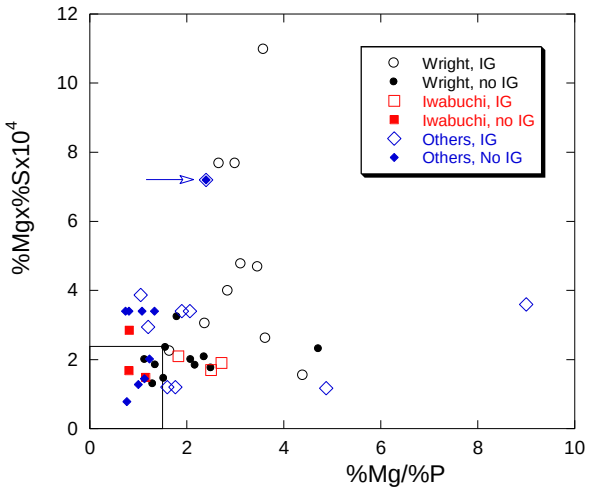

Figure 9. Plot of %Mg·%S versus %Mg/%P of SGI alloys showing (open symbols) or no (solid symbols) IG fracture. Data from Wright and Farrell [6], Iwabuchi and Kobayashi [15], and other works (see text).

4.2 Mechanism for ITB

In addition to an extended series of tensile tests under air, Wright and Farrell [6] carried out a few tests under a 10^{-3} Pa vacuum at 425°C and observed no IG fracture for alloys that were sensitive to ITB under air, namely their alloys E, B and G as described in Appendix A. The authors recognized they could not explain this result with the embrittling mechanism assuming sulfur diffusion that they considered based on its known effect in steels at low temperature. Further, the alloys studied by Wright and Farrell contained also phosphorus that is known to compete for grain boundary

segregation with sulfur [25]. Hence, if the sulfur content is increased, it may be expected it will overcome the repelling effect of phosphorus, and vice versa. As a matter of fact, what we can conclude is that not only sulfur but also magnesium and phosphorus do not embrittle SGI on their own in between 350°C and 500°C.

A further remark concerns magnesium that is expected to be one of the most potential elements to decrease the strength of grain boundaries according to the theoretical approach of Seah [26] that has already been referenced by Hung-Mao Lin et al. [27] in the context of SGI. However, magnesium is not known to segregate to grain boundaries, i.e., elemental magnesium at grain boundaries has not been reported at level that would suggest grain boundary segregation. In agreement with this latter statement, all observations of magnesium rich areas at the grain boundaries or fracture surface of SGI show it associated with other elements, in particular oxygen and phosphorus [7, 24, 28].

Based on the above remarks and the results of this work, it is quite straightforward to propose a mechanism for ITB of as-cast SGI. During tensile or other mechanical testing under air, oxygen penetrates through the grain boundaries leading to precipitation of MgO. As the temperature of the test increases, the amount of oxygen that enters the material and diffuses into it increases, and the size and number of MgO particles increase accordingly. When the test temperature has reached 300-350°C, the size of these particles gets higher than the critical size for initiating grain boundary defects and the ductility starts decreasing with the appearance of IG fracture. As the temperature increases, IG failure becomes more and more frequent up to 500°C; beyond that, the decrease in ferrite grain strength does not allow the critical stress for IG failure to be reached so that ductility is recovered.

The above mechanism is sustained by two further observations reported in the literature. First, ITB is sensitive to the strain rate, the ductility minimum being displaced to higher temperature when the strain rate is increased [10, 6, 15]. As pointed out by Wright and Farrell [6], this is a strong indication that the phenomenon is, at least partly, controlled by diffusion. While Wright and Farrell considered sulfur as the diffusing species, it appears more probable that this is oxygen as discussed above. Also, Yanagisawa and Lui [5] studied the effect of the ferrite grain size by

varying the casting dimensions. The elongation at rupture increased with the grain size from RT to 200°C, but then decreased and at 400°C the two casts with largest ferrite grain size showed IG whilst those with the smallest ferrite grain size did not (their figure 5). This could possibly be attributed to a blocking effect of the grain boundaries, but could as well be indicative of grain boundary diffusion that is retarded by smaller grain size because of the lengthening of the diffusion path.

It has been noted that most of the literature results discussed in this work refer to materials that have been heat treated to ensure a fully ferritic matrix. It is quite possible that oxygen entered these materials during the heat treatment, leading to the Mg-rich precipitates that were observed. In turn, heavy section castings in which large stresses develop during cooling could be susceptible to ITB as the shake-out operates in the 300-500°C temperature range. Such an effect could be more pronounced in high silicon SGI because the chemical ordering of ferrite begins in the same temperature range.

Conclusion

The present study showed the presence of MgO precipitates on the intergranular facets of the fracture surface of tensile specimens tested between room temperature and 650°C, obtained from an as-cast high-silicon spheroidal graphite cast iron. The size of these precipitates increases significantly with test temperature, indicating that IG fracture-related embrittlement is controlled by oxygen ingress from ambient air. This analysis is supported by a number of other observations reported in the literature, such as the fact that ferritic SGI are immune to embrittlement when tested in vacuum. Further studies in this area should be devoted to the beneficial effect of phosphorus on the intermediate temperature embrittlement of ferritic SGI.

Data availability statement

Raw data (strain/stress curves) are available on request to the authors

Funding

This research did not receive any specific grant from funding agencies in the public, commercial, or not-for-profit sectors.

References

[1] Lei Zheng, G. Schmitz, Ye Meng, R. Chellali, R. Schlesiger, Mechanism of intermediate temperature embrittlement of Ni and Ni-based superalloys, Critical Reviews in Solid State and Materials Sciences, 37, 2012, 181-214. DOI: 10.1080/10408436.2011.613492

[2] W.T. Lankford, Some considerations of strength and ductility in the continuous-casting process, Metall. Trans. 3, 1972, 1331-1357. DOI: 10.1007/BF02643017

[3] B. Mintz, The influence of composition on the hot ductility of steels and to the problem of transverse cracking, ISIJ Int., 39, 1999, 833-855. DOI: 10.2355/isijinternational.39.833

[4] B. Mintz, D.N. Crowther, Hot ductility of steels and its relationship to the problem of transverse cracking in continuous casting, Inter. Mater. Rev., 55, 2010, 168-196. DOI: 10.1179/095066009X12572530170624

[5] O. Yanagisawa, T. S. Lui, Influence of the structure on the 673 K embrittlement of ferritic spheroidal graphite cast iron, Transaction of the Japan Institute of Metals, 24, 1983, 858-867. DOI: 10.2320/matertrans1960.24.858

[6] R.N. Wright and T.R. Farrell, Elevated temperature brittleness of ferritic ductile iron, *AFS Trans.*, 93, 1985, 853-66.

[7] S.F. Chen, T.S. Lui, L.H. Chen, The effect of phosphorus segregation on the intermediate-temperature embrittlement of ferritic, spheroidal graphite cast iron, Metall. Mater. Trans., 25A, 1994, 557-561. DOI: 10.1007/BF02651597

[8] S.F. Chen, T.S. Lui, L.H. Chen, The role of magnesium-containing spheroidizer and counteraction of misch metal in the intermediate temperature intergranular embrittlement of ferritic nodule iron, Metall. Mater. Trans., 25A, 1994, 2305-2309.

[9] T. S. Lui, C. G. Chao, High-temperature properties of ferritic spheroidal graphite iron, Journal of Materials Science, 24, 1989, 2503-2507. DOI: 10.1007/BF01174520

[10] T. Kobayashi, K. Nishino, Y. Kimoto, Y. Awano, Y. Hibino, H. Ueno, 673K embrittlement of ferritic spheroidal graphite cast iron by magnesium. Journal of Japan Foundry Engineering Society, 70, 1998, 273-278. DOI: 10.11279/jfes.70.273

[11] F.T. Shiao, T.S. Lui, L.H. Chen, S.F. Chen, Eutectic cell wall morphology and tensile embrittlement in ferritic spheroidal graphite cast iron, Metall. Mater. Trans., 30A, 1999, 1775-1784. DOI: 10.1007/s11661-999-0176-8.

[12] M. Takanezawa, Y. Kobayashi, Y. Tomota, Fracture mechanism and suppression method of 673 K embrittlement in spheroidal graphite cast iron, Journal of JFS, 69, 1997, 41-48. DOI: 10.11279/jfes.69.41
[13] C.G.Chao, T.S.Lui, M.H.Hon, The effect of microstructure of ferritic spheroidal graphite cast irons on intergranular fracture at intermediate temperatures, Metall. Trans., 20A, 1989, 431-436. DOI: 10.1007/BF02653922
[14] Y. Iwabuchi, I. Kobayashi, H. Narita, Prevention of elevated temperature brittleness in ferritic ductile iron by phosphorus, J. JFS 69, 1997, 304-308. DOI: 10.11279/jfes.69.304
[15] Y. Iwabuchi, I. Kobayashi, Suppression of elevated temperature brittleness in spheroidal graphite cast iron by increasing phosphorus content, Key Eng. Mater. 457, 2011, 428-432. DOI: 10.4028/www.scientific.net/KEM.457.428
[16] E. Garcia Trelles, S. Eckmann, C. Schweizer, Experimental characterization of the short crack growth behavior of a ductile cast iron (DCI GJS-500) affected by intergranular embrittlement at temperatures nearby 400°C, Int. J. Fatigue, 155, 2022, 106573. DOI: 10.1016/j.ijfatigue.2021.106573
[17] R. González-Martínez, U. de la Torre, A. Ebel, J. Lacaze, J. Sertucha, Effects of high silicon contents on graphite morphology and room temperature mechanical properties of as-cast ferritic ductile cast irons. Part II – Mechanical properties, Materials Science and Engineering A, 712, 2018, 803-811. https://doi.org/10.1016/j.msea.2017.11.051
[18] J. Laine, K. Jalava, J. Vaara, K. Soivio, T. Frondelius, J. Orkas, The mechanical properties of ductile iron at intermediate temperatures: The effect of silicon content and pearlite fraction, International Journal of Metalcasting, 15, 2021, 538-547. DOI: 10.1007/s40962-020-00473-8.
[19] K. Avery, J. Pan, C. Engler-Pinto, Effect of temperature cycle on thermomechanical fatigue life of a high silicon molybdenum ductile cast iron, SAE Technical Paper 2015-01-0557. DOI:10.4271/2015-01-0557
[20] C.P. Cheng, T.S. Lui, L.H. Chen, Effect of residual magnesium contento n termal fatigue cracking behavior of high-silicon spheroidal graphite cast iron, Metall. Mater. Trans., 30A, 1999, 1549-1558. DOI: 10.1007/s11661-999-0092-y

[21] I. Hervas, A. Thuault, E. Hug, Damage analysis of ferritic SiMo ductile cast iron submitted to tension and compression loadings in temperature, Metals, 5, 2015, 2351-2369. DOI: 10.3390/met5042351
[22] D. Li, C. Sloss, Brittleness at medium temperature of spheroidal graphite, mixed graphite, and compacted graphite high-silicon molybdenum cast irons, AFS Proceedings, 2015, paper 15-018
[23] M. Takanezawa, Y. Tomota, Y. Kobayashi, A new heat resistant cast iron for thin wall exhaust manifold, ISIJ Int., 38, 1998, 106-108. DOI: 10.2355/isijinternational.38.106
[24] O. Yanagisawa, H. Ishii, K. Matsugi, T. Hatayama, 673 K embrittlement of ferritic spheroidal graphite cast iron with low residual magnesium content, J. JFS 72, 2000, 604-609. DOI: 10.11279/jfes.72.604
[25] C.L. Briant, Competitive grain boundary segregation in Fe-P-S and Fe-P-Sb alloys, Acta metal., 36, 1988, 1805-1813. DOI: 10.1016/0001-6160(88)90249-0
[26] M.P. Seah, Adsorption-induced interface decohesion, Acta metal. 28, 1980, 955-962. DOI: 10.1016/0001-6160(80)90112-1
[27] Hung-Mao Lin, Truan-Sheng Lui, Li-Hui Chen, Effect of maximum temperature on the cyclic-heating-induced embrittlement of high-silicon ferritic spheroidal-graphite cast iron, Mater. Trans. 45, 2004, 569-576. DOI: 10.2320/matertrans.45.569
[28] S.N. Lekakh, C. Johnson, A. Bofah, L. Godlewski, Mei Li, Improving high-temperature performance of high Si-alloyed ductile iron by altering additions, Int. J. Metalcasting, 15, 2021, 874-888. DOI: 10.1007/s40962-020-00524-0

Appendix A. Details about the data from Wright and Farrell.

Amongst the many alloys studied by Wright and Farrell [WR85], those with fully spherical graphite as indicated in their Table 2 were selected for figure 9. These are alloys with a silicon content varying from 2.12 wt.% to 3.30 wt.%. All alloys had been submitted to tensile testing at room temperature and at 425°C, at a strain rate of $8.3 \cdot 10^{-5}$ s^{-1} up to yielding, followed by a strain rate of $8.3 \cdot 10^{-4}$ s^{-1} to fracture. The alloys were differentiated as showing or not IG on the basis of the RA values listed in Appendix A of the Wright and Farrell paper.

Wright and Farrell selected four alloys (labeled B, E, G and H) whose composition is listed in Table A1 below that they submitted to several test temperatures from RT to 650°C. These results were used for plotting Figure 1 of the main text. A particularly interesting experiment carried out by Wright and Farrell consisted in performing trials at 425°C under vacuum. This was done on alloys B, E and G and the values of UTS and RA under this condition are compared to the values under ambient air in Figure A1. It is seen that UTS and RA values are higher under vacuum and the authors noticed that all three samples were immune to IG.

Table A1. Composition of four of the alloys studied by Wright and Farrell (wt.%). Other elements that could be present at low level were Ti, V, Al, Cu and Cr. The heat treatment (HT) is indicated in the second column: FA: full anneal; SCA: sub-critical anneal.

Heat	HT	C	Si	Ni	Mo	Mn	P	Mg	S
B	FA	3.60	2.20	0.38	0.74	0.23	0.018	0.048	0.016
E	FA	3.70	2.18	0.15	0.67	0.19	0.016	0.048	0.016
G	SCA	3.43	2.21	1.23	0.40	0.09	0.017	0.053	0.009
H	SCA	3.55	2.63	0.13	0.61	0.09	0.017	0.023	0.008

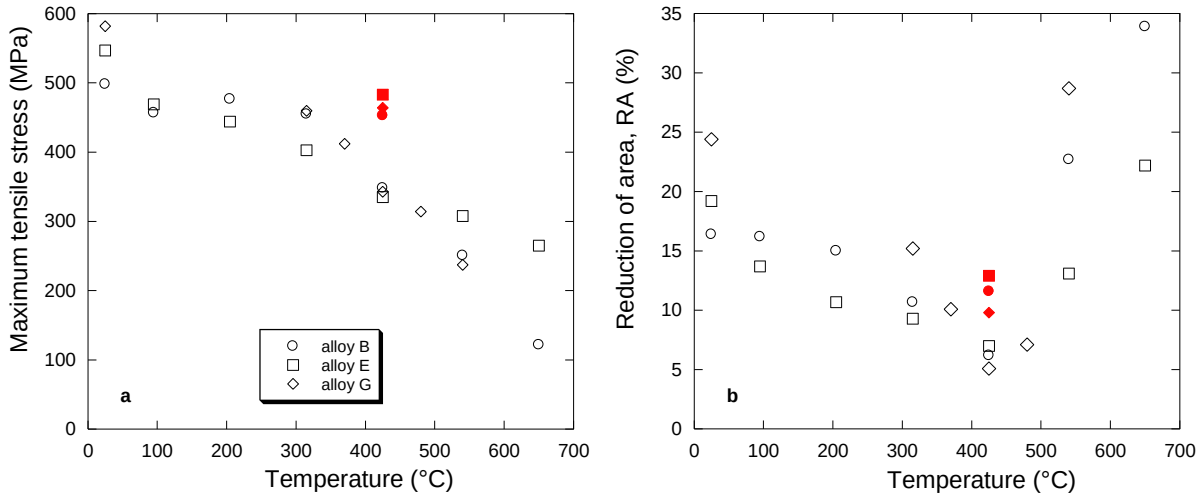

Figure A1. Evolution with temperature of the UTS (a) and of the reduction of area at rupture RA (b) for the alloys B, E and G studied by Wright and Farrell [6]. Open symbols are for test under ambient air and solid symbols for trials under vacuum. Whenever there were duplicate values, this is the mean that is plotted.

Appendix B

Attempt has been carried out to characterize the composition of the particles using EDS. Owing to their small size, at most 200 nm when the electron beam of the SEM is of the order of 1 µm in diameter, the EDS spectra were expected to show signal coming from both the pointed particle and the matrix around it. The spectra shown in Figures B1 (sample ruptured at 100°C), Figure B2 (sample ruptured at 450°C) and Figure B3 (sample ruptured at 500°C) do all show a peak corresponding to O and a small one associated to Mg in addition to the peaks of C, Fe and Si. It has been verified that the Mg peak does not appear when the EDS spectra is accumulated on the matrix while the O peak is generally smaller in those locations. It can thus be claimed with some confidence that the particles were MgO precipitates.

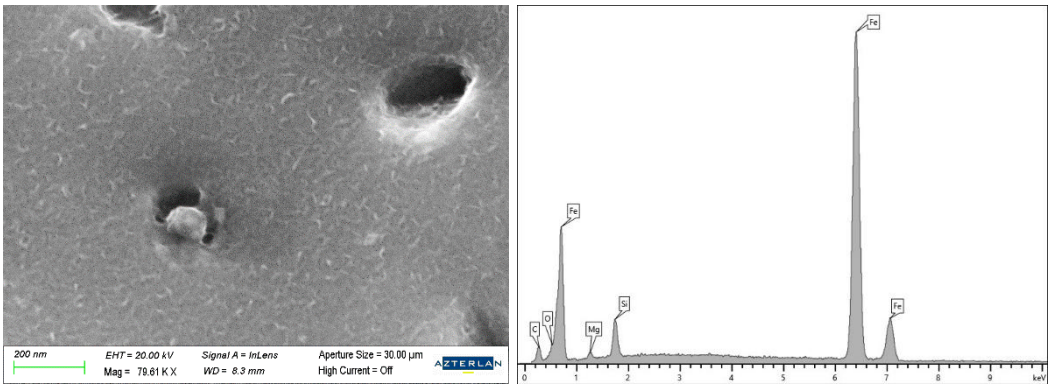

Figure B1. SEM micrograph and EDS spectrum with the beam focused on the round particle in the center of the field. Sample ruptured at 100°C.

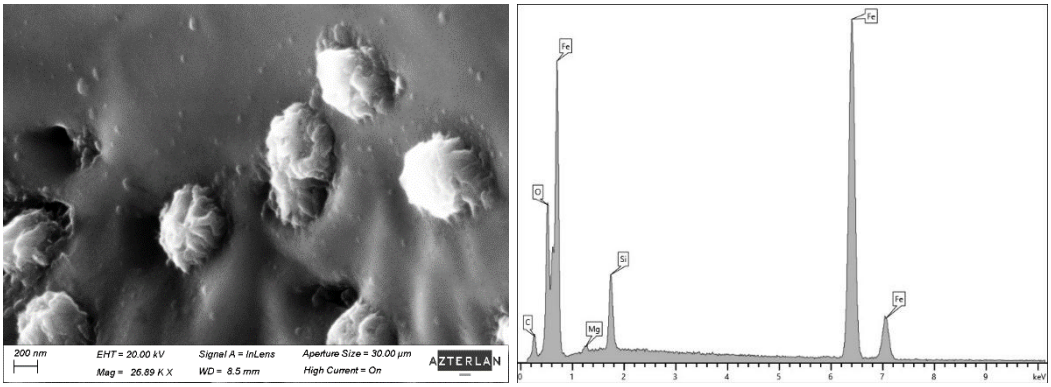

Figure B2. SEM micrograph and EDS spectrum with the beam focused on the particle in the center of the field. Sample ruptured at 450°C.

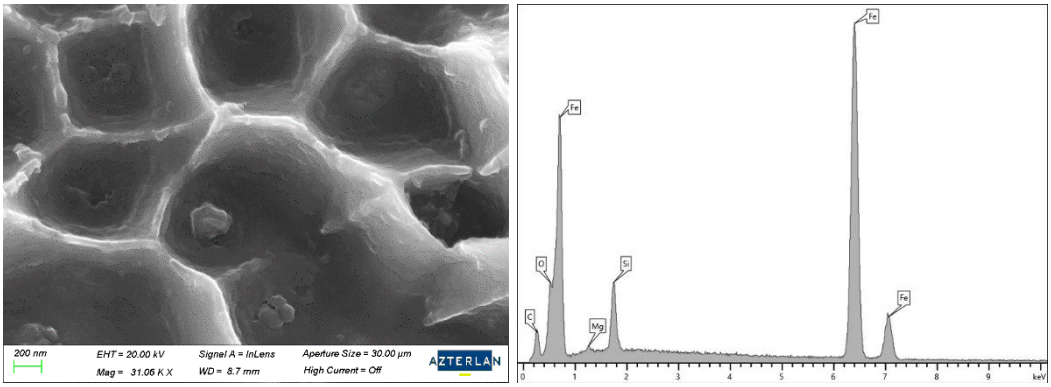

Figure B3. SEM micrograph and EDS spectrum with the beam focused on the particle in the center of the field. Sample ruptured at 500°C.